THE JOURNAL OF PHYSICAL CHEMISTRY C

Article

pubs.acs.org/JPCC

Fast Charge-Carrier Trapping in TiO_2 Nanotubes

C. Wehrenfennig,[†] C. M. Palumbiny,[‡] H. J. Snaith,[†] M. B. Johnston,[†] L. Schmidt-Mende,[¶] and L. M. Herz*,[†]

[†]Oxford University, Clarendon Laboratory, Parks Road, Oxford OX1 3PU, United Kingdom

[¶]Universität Konstanz, Fachbereich Physik, Postfach M680, 78457 Konstanz, Germany

ABSTRACT: One-dimensional semiconductors such as nanowires and nanotubes are attractive materials for incorporation in photovoltaic devices as they potentially offer short percolation pathways to charge-collecting contacts. We report the observation of free-electron lifetimes in TiO_2 nanotubes of the order of tens of picoseconds. These lifetimes are surprisingly short compared to those determined in films of TiO_2 nanoparticles. Samples of ordered nanotube arrays with several different tube wall thicknesses were fabricated by anodization and have been investigated by means of optical-pump-terahertz-probe (OPTP) spectroscopy, which allows measurement of transient photoinduced conductivity with picosecond resolution. Our results indicate a two-stage decay of the photoexcited electron population. We attribute the faster component to temporary immobilization of charge in shallow trap states, from which electrons can detrap again by thermal excitation. The slower component most likely reflects irreversible trapping in states deeper below the conduction band edge. Free-electron lifetimes associated with shallow trapping appear to be independent of the tube wall thickness and have very similar values for electrons directly photoexcited in the material and for those injected from an attached photoexcited dye. These results suggest that trap states are not predominantly located at the surface of the tubes. The effective THz charge-carrier mobility in the TiO_2 nanotubes is determined (0.1−0.4 $cm^2/(Vs)$) and found to be within the same range as carrier mobilities reported for TiO_2 nanoparticles. Implications for the relative performance of these nanostructures in dye-sensitized solar cells are discussed.

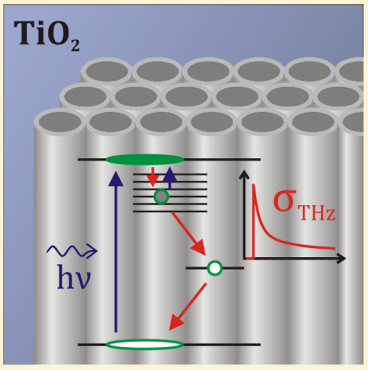

INTRODUCTION

Nanostructures of titanium dioxide are intensely studied with respect to their use in a wide range of applications including photocatalysts,[1] energy storage,[2] and photovoltaics.[3,4] This article devotes particular attention to TiO_2 nanotube arrays employed as an anode material in dye-sensitized solar cells (DSCs). One of the crucial properties for this application is charge-carrier conductivity, which undergoes tremendous changes at the transition from bulk single crystals to a nanostructured material.[5] Current record efficiency DSCs are based on sintered (anatase-)TiO_2 nanoparticles,[6] for which global DC mobility values between 7×10^{-6} $cm^2/(Vs)$ (from time-of-flight measurements[5]) and 1.7×10^{-2} $cm^2/(Vs)$ (from transient photocurrent measurements on DSCs[7]) have been reported. These lie at least 3 orders of magnitude below the corresponding value for bulk single crystals of 10 $cm^2/(Vs)$ (from Hall effect measurements[8]). Only because of the very long recombination lifetime of injected electrons in TiO_2 with the oxidized dye or the hole transporter do such DSCs have a sufficiently high diffusion length for electrons to reach the contacts with close to 100% probability.[9] However, this lifetime critically depends on the composition of the cell, and, particularly in solid state DSCs, where interfacial electron−hole recombination has been found to be much faster than in liquid electrolyte cells,[10,11] higher charge-carrier mobilities are required in order to achieve highly efficient charge collection. Interestingly, measurements of the early time, local (intra-particle) charge-carrier mobility in TiO_2 nanoparticle films using optical-pump-THz-probe (OPTP) spectroscopy yielded values of between 10^{-2} $cm^2/(Vs)$ and 10^{-1} $cm^2/(Vs)$.[12,13] In fact, taking electric field screening due to the high dielectric constant of TiO_2 into account, accordingly corrected values approach THz mobilities obtained on (rutile-)TiO_2 single crystals of 1 $cm^2/(Vs)$.[14] This led to the conclusion that the low global carrier mobilities in TiO_2 nanoparticle films can be attributed to slow interparticle transfer.[7,12,15]

In order to reduce the number of interparticle transfers and to provide a more direct precolation path for electrons from the point of excitation to the contacts, 1D structures have been used in DSCs,[16−18] most notably nanotubes. With anodization, a relatively simple and scalable fabrication technique exists for films of highly ordered TiO_2-nanotube-arrays.[19] Unfortunately, the performance of nanotubes in DSCs has up to now proved to be inferior to the performance of those based on nanoparticles.[4] Although a reduction in overall power conversion efficiency could be attributed to a reduction in specific surface area, it is surprising that not even an increase in charge collection rate has been observed.[17,20] Here we present a study based on optical pump terahertz probe experiments on TiO_2 nanotubes, which indicates that fast trapping immobilizes carriers on time scales of a few tens of picoseconds—about an order of magnitude faster than the early time free carrier decay

Received: February 25, 2015
Revised: March 31, 2015
Published: April 7, 2015

DOI: 10.1021/acs.jpcc.5b01827
J. Phys. Chem. C 2015, 119, 9159−9168

observed in sintered nanoparticle films at similar photoexcitation density. The observations are interpreted within a model involving energetically shallow traps, from which thermal detrapping is possible, and energetically deep traps, which irreversibly immobilize carriers. In addition, we examine the influence on trapping lifetimes of the wall thickness of the tubes, which can be varied through temperature control of the anodization bath. Finally, we discuss how such trapping effects may influence the charge-carrier transport in devices.

EXPERIMENTAL DETAILS

Samples. TiO_2 nanotube films were prepared on quartz substrates by anodization of titanium at different temperatures and subsequent annealing. The substrates were cleaned in ultrasonic baths of acetone and isopropanol for 30 min each and by oxygen plasma treatment. Using a Surrey Nano-Systems Gamma 1000C sputter coating system, approximately 1 μm of Ti was DC sputtered at 500 °C under an Ar atmosphere at a pressure of 4 mTorr. Afterward, the samples were allowed to cool down slowly under high vacuum. Anodization was performed in an ethylene glycol bath with 0.3 wt % NH_4F (Sigma-Aldrich) using a Pt counter electrode.

Two batches of samples were anodized at a range of temperatures T_{ano} between 5 and 55 °C in steps of 10 °C, at an anodization voltage of 20 V and for durations between 1 min and 2 h. Afterward, the samples were rinsed with water and ethanol and dried in air. Because anodization produces amorphous nanotubes, the films were annealed to obtain polycrystalline material. Annealing of the first batch was performed by ramping the temperature up to 450 °C at a heating rate of 3 °C/min in ambient atmosphere under observation by means of in situ X-ray. The second batch was annealed for 3 h at 310 °C, which is closely above the crystallization temperature of the anatase phase as verified using XRD.

At a subsequent stage, the nanotubes were covered in a monolayer of a ruthenium-based dye (Z907) by immersion in a solution of 3 mg of Z907 in 20 mL of ethanol for 18 h. (The terms *undyed* and *dyed* are used in this article to distinguish between the state of the samples before and after this processing step.) In preparation for the dye attachment, the films were heated up to 200 °C in order to remove any surface-adsorbed water. After immersion, excess dye was removed by cleaning the samples in acetonitrile. Finally, the dye was removed from one batch of samples again by immersion in base (KOH in ethanol) for 5 h. These samples were then cleaved and sputter-coated in 2 nm of Pt for scanning electron microscopy (SEM) imaging.

A set of reference samples of 20 nm TiO_2 nanoparticles have been prepared by spin-coating a 1:1.5 solution of Dyesol nanoparticle paste in ethanol at 1000 rpm for 10 s followed by 2000 rpm for 40s on a quartz substrate. The films were then dried and sintered for 30 min at 450 °C. The thickness of the reference samples is about 3 μm, as determined by surface profiling.

Scanning Electron Microscopy (SEM). Top-view and cross-sectional SEM images were taken of all samples of the first batch (annealed at 450 °C) after all spectroscopic experiments were completed. A Hitachi S-4300 microscope was used at an acceleration voltage of 5 kV, an emission current of 10 μA, and 14 mm working distance.

THz Time-Domain Spectroscopy. THz time domain spectroscopy (THz-TDS) is a powerful probe for the investigation of ultrafast charge carrier dynamics and as a contactless technique particularly well suited for the study of nanostructured materials.[13,21−23] By scanning the full waveform of a THz pulse transmitted through the sample, the full complex dielectric function in the range from a few hundred gigahertz to a few terahertz can be directly reconstructed. In an optical-pump-terahertz-probe (OPTP) configuration, the sample is excited by an optical pulse and then probed by a terahertz pulse after a well-defined delay. This allows the study of charge-carrier dynamics, such as charge injection, trapping, and recombination with picosecond time-resolution.[24,25]

For measurements presented in this study, we used a Ti:Saphire regenerative amplifier to generate 40 fs pulses at 800 nm wavelength and a repetition rate of 1.1 kHz. Terahertz pulses are generated by optical rectification in a 2 mm-thick ZnTe crystal and detected by electro-optic sampling in another ZnTe crystal of 0.2 mm thickness. We excited undyed TiO_2-nanotubes directly at a wavelength of 266 nm corresponding to a photon energy of 4.66 eV, which is well above the bandgap of anatase-TiO_2 (3.2 eV[26,27]). Pulses of this wavelength are generated by third harmonic generation (THG)[28] of the laser output. Dyed samples on the other hand were excited at 545 nm using the output of an optical parametric amplifier (OPA). The corresponding photon energy of 2.27 eV lies well below the bandgap of anatase, but at the same time, it is strongly aborbed by the dye Z907. If not explicitly stated otherwise, measurements have been performed with the sample in an evacuated chamber, at a pressure in the range of 10^{-2} mbar to 10^{-1} mbar.

RESULTS AND DISCUSSION

Figure 1a shows an SEM cross-sectional image of a typical nanotube film. The most notable feature is that the morphology of the tubes differs from the top, where the surface is smooth, to the bottom, where the tubes exhibit periodic rings. This phenomenon can be observed on all samples with the exception of the one anodized at 55 °C and has been reported before by several groups.[19,29] Such rings have been associated with regular current fluctuations, the occurrence and amplitude of which depends on the acid concentration in the anodization bath.[30] A typical top-view SEM image of a nanotube film is shown in Figure 1b. Analysis of the full set of images reveals a pore-to-pore distance of about 80 nm (which is independent of the tube wall thickness as reported in ref 31) and tube lengths between 1 and 2 μm for all samples.

As a starting point for the study of the early time carrier decay dynamics in TiO_2 nanotubes, we recorded the excitation-density dependence of the transient THz photoconductivity. Previous reports have already shown that the response of photoexcited TiO_2 to a THz probe[13,14] or a microwave probe[32] is dominated by the contribution from electrons. Further evidence for this will also be presented later in this article.

Trapping and Detrapping Dynamics in Undyed Nanotubes. Figure 2 shows the photoinduced THz response of a TiO_2 nanotube film as a function of time after excitation with fluences between 13 μJ/cm^2 (1.7×10^{13} photons/cm^2) and 126 μJ/cm^2 (1.7×10^{14} photons/cm^2). Here, the term *THz response* is used in short for the change in electric field transmission, which is proportional to the conductivity of the probed thin film and hence to the product of free charge-carrier density n and mobility μ.

In general, changes in both charge-carrier mobility and concentration determine the shape of the THz transmission

DOI: 10.1021/acs.jpcc.5b01827
J. Phys. Chem. C 2015, 119, 9159−9168

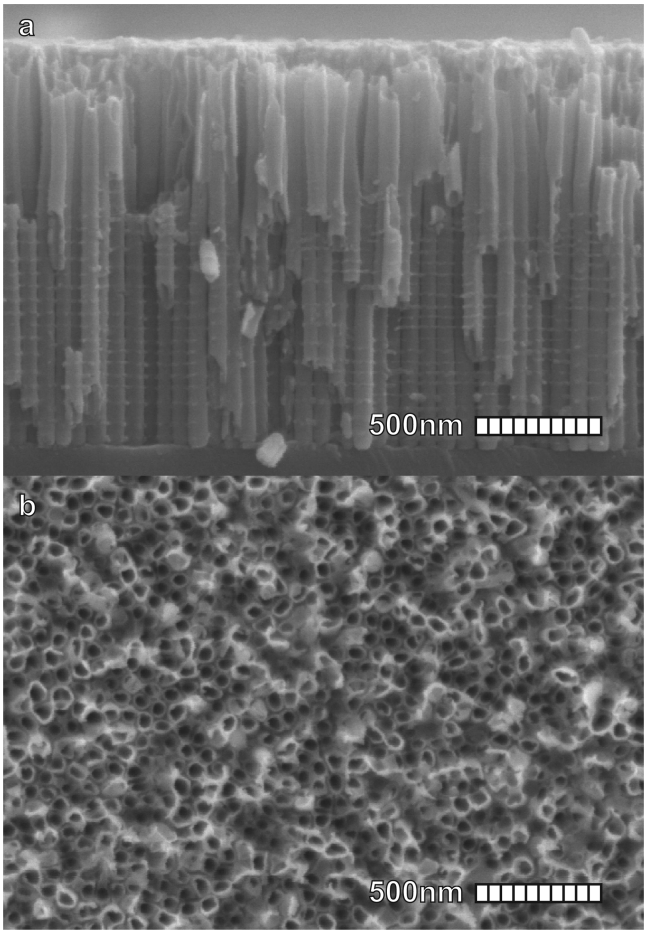

Figure 1. Typical SEM images of TiO_2 nanotube samples used in this study in (a) cross-sectional and (b) top view. The images have been taken at an acceleration voltage of 5 kV after sputtering a 2 nm layer of platinum onto the samples.

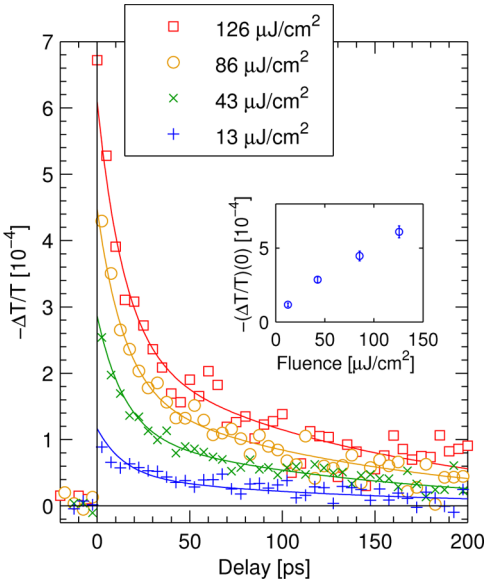

Figure 2. THz transmission transients (266 nm excitation in vacuum) of undyed TiO_2 nanotubes (T_{ano} = 5 °C) for a range of excitation fluences. Symbols: experimental data. Lines: simultaneous fits to eq 2 as described in the text. Inset: amplitudes of the initial THz response vs excitation fluence.

transient. However, the most plausible cause for the partially rapid dynamics displayed by the curves in Figure 2 is a decay of free carrier population through mechanisms such as trapping or recombination. This interpretation is supported by the observation that THz photoconductivity spectra (presented later) do not change as a function of time after photoexcitation. If there was a change of the intrinsic mobility on the investigated time scale (e.g., due to carrier-cooling effects or a reduced influence of carrier−carrier scattering processes), its frequency dependence would be likely to change as well. Here, we therefore make an approach to interpret the THz transmission transients on the assumption that their shape is predominantly determined by the decay of carrier concentration while the carrier mobility is taken to be constant, at least over the picosecond-to-nanosecond observation window. The most striking feature of the data in Figure 2 is a rapid population decay within tens of picoseconds irrespective of the excited carrier density, which indicates that it arises from a monomolecular process such as carrier trapping. The data additionally shows a longer-lived component; hence a simple monoexponential decay function alone does not provide an adequate model for extraction of physically sensible lifetimes. Bimolecular effects on the other hand such as free electron−hole recombination can be ruled out as these would require that the initial slope of the decay curve scales with excitation density.

It has been well established that charge transport in nanostructured TiO_2 is inhibited by frequent trapping−detrapping events.[33−36] Such trapping events are very likely to be reflected in the transient THz response as already observed for TiO_2 nanoparticles.[13] Further studies on nanoparticles using photoluminescence and visible/IR transient absorption[37,38] have suggested that the carrier recombination process also involves energetically deep trap sites assignable to surface states or defects such as oxygen vacancies,[39,40] to which shallowly trapped carriers can transfer, but from which no thermal escape is possible. On the basis of these insights, we formulate a model which describes the observed decay dynamics in terms of trapping, detrapping, and deep-trapping processes as expressed by the following equations:

$$\frac{\mathrm{d}}{\mathrm{d}t}n_{\mathrm{free}}(t) = -k_{\mathrm{trap}}n_{\mathrm{free}}(t) + k_{\mathrm{detrap}}n_{\mathrm{trapped}}(t) - k_{\mathrm{deep}}n_{\mathrm{free}}(t)$$
$$\frac{\mathrm{d}}{\mathrm{d}t}n_{\mathrm{trapped}}(t) = k_{\mathrm{trap}}n_{\mathrm{free}}(t) - k_{\mathrm{detrap}}n_{\mathrm{trapped}}(t) - k_{\mathrm{deep}}n_{\mathrm{trapped}}(t) \quad (1)$$

Here, n_{free} is the density of free electrons and n_{trapped} the density of electrons in shallow traps. Furthermore, k_{trap} represents the shallow-trapping rate, k_{detrap} the detrapping rate (from shallow traps), and k_{deep} the deep-trapping rate. This system of equations can be solved analytically, resulting in a biexponential expression for the free-electron density:

$$n_{\mathrm{free}}(t) = \frac{n_{\mathrm{free}}(0)}{k_{\mathrm{trap}} + k_{\mathrm{detrap}}}(k_{\mathrm{trap}}\, e^{-(k_{\mathrm{detrap}}+k_{\mathrm{trap}}+k_{\mathrm{deep}})t} + k_{\mathrm{detrap}}\, e^{-k_{\mathrm{deep}}t})$$
$$n_{\mathrm{trapped}}(t) = \frac{n_{\mathrm{free}}(0)}{k_{\mathrm{trap}} + k_{\mathrm{detrap}}}(-k_{\mathrm{trap}}\, e^{-(k_{\mathrm{detrap}}+k_{\mathrm{trap}}+k_{\mathrm{deep}})t} + k_{\mathrm{trap}}\, e^{-k_{\mathrm{deep}}t}) \quad (2)$$

DOI: 10.1021/acs.jpcc.5b01827
J. Phys. Chem. C 2015, 119, 9159−9168

We simultaneously fitted this solution to the THz photoconductivity transients for all excitation fluences (i.e., the entire data set shared a single common fit parameter for each rate constant). Figure 2 displays this fit as solid lines showing that these are able to reproduce the shape of the decays well. The resulting rate constants, expressed in terms of lifetimes are $\tau_{trap} = 1/k_{trap} = (27 \pm 6)$ ps, $\tau_{detrap} = 1/k_{detrap} = (43 \pm 10)$ ps, and $\tau_{deep} = 1/k_{deep} = (140 \pm 16)$ ps. In the scenario described by the model, the simultaneous processes of trapping and detrapping lead to a relaxation into an equilibrium. Eventually, on a longer time scale, all carriers are immobilized irreversibly in deep traps.

In the next step, we compare the observed carrier recombination dynamics in TiO_2 nanotubes to those in sintered TiO_2 nanoparticles. Figure 3 displays THz photoconductivity transients for both morphologies. It is immediately visible that under comparable excitation conditions, the early time decay of the free electron population is at least an order of magnitude faster in the nanotubes, which suggests a much higher density of trap states present in this material.

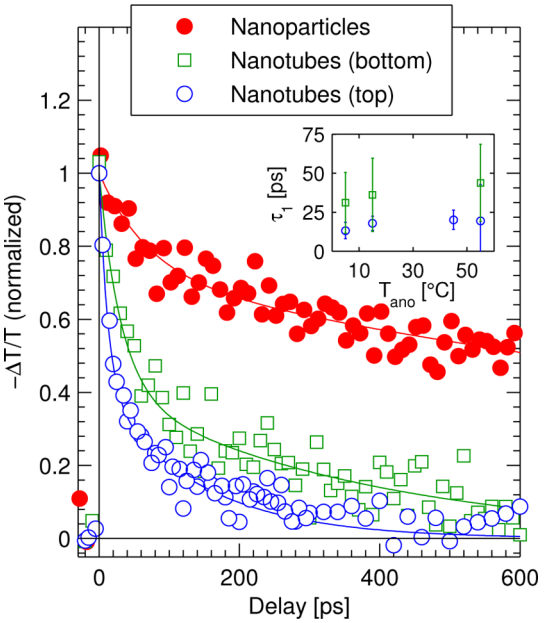

Figure 3. THz transmission transients ($-dT/T$, normalized) after excitation with a 40 fs/266 nm light pulse in vacuum. Open circles: TiO_2 nanotubes (T_{ano} = 5 °C, undyed, excitation fluence: 125 μJ/cm^2), excited from their free side. Open squares: TiO_2 nanotubes (T_{ano} = 5 °C, undyed, excitation fluence: 100 μJ/cm^2), excited from the substrate side. Closed circles: sintered TiO_2 nanoparticles (Dyesol, 20 nm, undyed, excitation fluence: 125 μJ/cm^2). Lines: fits to eq 2 (biexponential) as described in the text. Inset: time constant $\tau_1 = (k_{trap} + k_{detrap} + k_{deep})^{-1}$ responsible for short initial decay of photoconductivity as extracted from fits for TiO_2 nanotubes anodized at different temperatures.

The variations in the fast-trapping lifetimes are compared between the top and the bottom part of the nanotubes as well as between samples with different tube wall thicknesses. A separate investigation of the top and bottom parts is possible because the absorption depth of the excitation light into the films is only about 70 nm compared to a film thickness of the order of 1 μm. (An absorption depth of ca. 35 nm has been reported for single crystalline anatase[41] and it is assumed that the absorbance approximately scales with the volume filling fraction of about 0.5 for the NT samples studied here.) As shown in Figure 3, slightly slower trapping ($\tau_{trap} = (57 \pm 40)$ ps) is found in the bottom parts. The inset compares the results from tubes grown at different anodization temperatures which exhibit a variation in tube wall thickness of over a factor of 2 as demonstrated in ref 31 (higher T_{ano} leads to thinner walls). A systematic dependence of lifetimes on wall thickness is not observed. In particular there is no indication that thinner walls (i.e., higher T_{ano}) lead to faster decay of charge conductivity as it may be expected for a predominant concentration of traps at the surfaces of the tubes and has been observed previously for semiconductor nanowires where surface trapping dominates.[42,43] The trend of slower trapping in the bottom parts of the tubes appears to occur independent of wall thickness. As the SEM image in Figure 1 indicates, the geometrical differences along the growth direction of the tubes are very small, hence an explanation for the change in trapping lifetime along the tubes is more likely to relate to the growth process itself. Such a connection could exist, for example, through the longer exposure of the top parts to the ammonium fluoride in the bath which may introduce impurities into the material[44,45] and could thereby create trap states. Alternatively, a variation in ionic concentrations in the bath during the anodization procedure could have a similar effect.

Effect of Ambient Air on Charge-Carrier Dynamics. Because it is well-known that exposure to oxygen can cause tremendous DC conductivity changes in TiO_2,[40,46] we performed measurements under ambient air in order to reveal its influence on the THz response. Unless explicitly stated otherwise, all other OPTP experiments have been performed under vacuum ($<10^{-1}$ mbar). The study of the influence of air is of additional value as it helps to ensure that our results are not significantly altered by effects of adsorbed gases that may remain on the nanotube surface for some time after the sample chamber is evacuated.

Measurements were taken in air at atmospheric pressure, at low vacuum (10^{-1} mbar), and at high vacuum ($\leq 10^{-4}$ mbar). Changes under exposure to the UV pump pulses were continuously monitored. We observed no changes in the THz transmission transients between a pressure of 10^{-1} mbar and even lower pressures (down to 10^{-5} mbar). However, comparing measurements taken in air at atmospheric pressure (~30% relative humidity) to those at 10^{-1} mbar or less as shown in Figure 4, we find that already during the first acquisition after exposure to atmospheric air, a long-lived component (with a lifetime much longer than the experimentally accessible 1.2 ns) emerges in the decay curves. Later, on time scales of tens of minutes to a few hours, it is also observed that the amplitude of the THz response decreases. This change is reversible on slightly longer time scales (several hours) through exposure to the 266 nm excitation light.

The interaction of ambient gases with TiO_2 surfaces is complex and has been the subject of numerous studies.[40,47,48] In particular, adsorbed oxygen has been found to cause tremendous changes to carrier dynamics in TiO_2 due to its ability to scavenge free electrons and thereby turn an oxygen-deficient n-doped surface into a p-doped surface. Desorption of oxygen can occur after electron capture and is hence facilitated by UV irradiation.[49] The observed drop in THz conductivity under air-exposure may be caused by a reduction of the incident photon-to-free-charge conversion ratio ϕ. This may occur through several potential mechanisms such as ultrafast immobilization of carriers on the sub-ps time scale, the emergence of additional absorbing states, and transitions

DOI: 10.1021/acs.jpcc.5b01827
J. Phys. Chem. C 2015, 119, 9159−9168

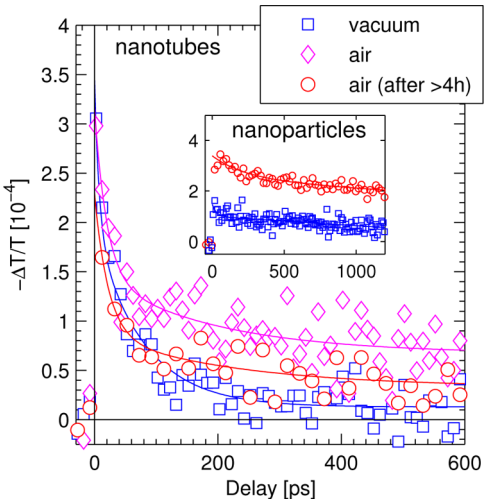

Figure 4. Comparison of THz transmission transients (266 nm excitation at fluence: 55 μJ/cm^2) of undyed TiO_2 nanotubes in vacuum (blue squares), immediately after exposure to air (pink diamonds), and after at least 4 h of exposure to air (red circles). Inset: result of the same experiment on sintered, undyed TiO_2 nanoparticles.

which do not lead to the creation of free charges. With respect to the slow emergence of a long-lived component under oxygen exposure, diffusion processes of oxygen (and titanium) atoms from and into the bulk of the material may cause changes of the concentration of deep trap states arising from oxygen vacancies.[40,50,51] The data obtained in this work is not sufficient to yield the exact mechanism causing the observed changes. However, with respect to the present study of electron lifetimes it is concluded that, in spite of the changes caused by the presence of air, the initial fast trapping process still appears to be active as the cause for the immobilization of a large part of the initial free carrier population on an unaltered time scale. In particular, we note that an influence of surface doping on fast trapping in TiO_2 nanotubes is therefore unlikely.

Charge-Carrier Dynamics in Dye-Sensitized Nanotubes. Up to this point, electrons were injected into the conduction band of TiO_2 nanotubes through direct excitation from the valence band by the pump pulse. We now turn our attention to dye-sensitized nanotubes as they would be used in actual dye-sensitized solar cells (i.e., excitation takes place in the dye and electrons are subsequently injected from the dye into the conduction band of the nanotubes).[52] A wavelength of 545 nm is chosen for photoexcitation of sensitized samples, which corresponds to a photon energy of 2.27 eV well below the bandgap of anatase TiO_2 to ensure that no direct excitation of the nanotubes occurs. The most important difference in this situation is that no holes are generated in the TiO_2, and recombination can only take place with the oxidized dye at the surface.

THz-conductivity decay curves on dyed samples are shown in Figure 5a for a range of excitation fluences. The fluence dependence of the signal amplitude (at zero pump−probe delay) is linear, indicating that charge injection is not limited by saturation effects within the employed range of excitation fluences. The shape of the decay curves closely resembles the dynamics measured for undyed nanotubes with the one notable difference that the conductivity does not fully decay to zero within the experimentally accessible time range of 1.2 ns (i.e., a very long-lived contribution remains). A similar behavior has also been observed in sintered nanoparticles.[13] For this work,

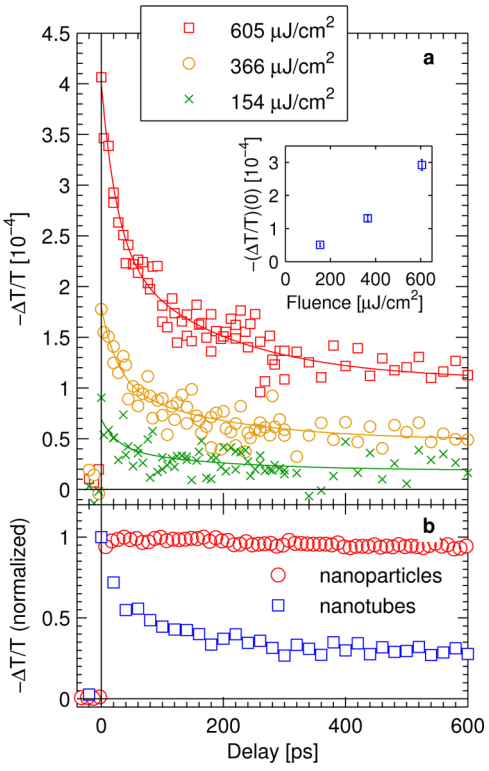

Figure 5. THz transmission transients (545 nm excitation, in vacuum) (a) of dye-sensitized TiO_2 nanotubes (T_{ano} = 5 °C) for different excitation fluences. Inset: amplitude of the initial THz response vs excitation fluence as extracted from fits (see text); (b) of dye-sensitized TiO_2 nanotubes (as in (a), highest fluence) in comparison to dye-sensitized, sintered TiO_2 nanoparticles (20 nm, Dyesol).

we also recorded data on dyed TiO_2 nanoparticles to serve as a reference measurement as shown in Figure 5b. In this figure, we do not observe any notable fast decay of the free-electron population.

The influence of dye-sensitization may be explained as follows: From photovoltage decay measurements it is known that recombination lifetimes of injected electrons with the oxidized dye are on the order of milliseconds or even seconds.[53,54] The excitation pulse repetition rate in experiments conducted here is 1.1 kHz (i.e., the time between subsequent pump−probe cycles is shorter than these lifetimes). Therefore, it can be expected that deep interband trap states which usually mediate recombination processes are gradually filled by injected electrons and hence passivated.[55] Consequently, an equilibrium between trapping and detrapping of electrons in shallow trap states is reached on a nanosecond time scale with a certain fraction of the initially excited carriers in the conduction band. Figure 6 gives a simplified illustration of the charge generation, injection, and recombination processes for undyed (Figure 6a) and dye-sensitized (Figure 6b) TiO_2 nanotubes as proposed and modeled here. In the case of nanoparticles, where the concentration of shallow traps was concluded to be significantly lower than in nanotubes, it appears to be possible that even these states are entirely passivated.

A comparison of conductivity decay in dyed and undyed samples (Figures 5 and 2) suggests similar trapping lifetimes and no dependence on excitation fluence for both systems. Sensible fitting of the data for the dyed case is difficult, because there might be injection dynamics on the ps-time scale superposing carrier decay processes.[13] However, in order to

DOI: 10.1021/acs.jpcc.5b01827
J. Phys. Chem. C 2015, 119, 9159−9168

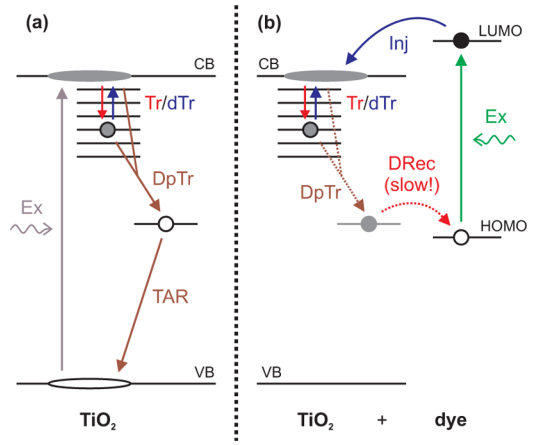

Figure 6. Illustration of processes within the model used in this study for charge-carrier dynamics in (a) undyed and (b) dye-sensitized TiO_2 nanotubes. Possible hole trapping processes are neglected here. The deep trap state in (b) is greyed out to depict that this state is almost permanently filled due to the recombination process with the oxidized dye (DRec) being much slower than the trapping process (DpTr). The corresponding recombination path is therefore very slow overall, as indicated by the dotted arrows. See text for details. Closed circles/ellipses: holes/normally unoccupied electron traps. Acronyms: CB: conduction band, DpTr: deep trapping, DRec: recombination with oxidized dye, dTr: (shallow) detrapping, Ex: (optical) excitation, HOMO: highest occupied molecular orbital, Inj: injection, LUMO: lowest unoccupied molecular orbital, TAR: trap-assisted recombination, Tr: (shallow) trapping, VB: valence band.

verify monomolecular decay behavior and to provide at least an estimate of the fast decay lifetime, we again apply biexponential fits according to eq 1—here with an additional constant contribution reflecting the long-lived electron population after saturation of all available deep trap states. All lifetimes and the relative magnitude of the long-lived component are shared among all transients for the different excitation fluences and globally optimized.

For the initial fast decay component (first term in eq 2), we obtain a time constant of 26 ps in comparison to 14 ps for undyed samples. The similarity of trapping times under direct excitation and after electron injection is worth noting as it suggests that shallow trap states occur homogeneously distributed throughout the bulk of TiO_2 nanotubes rather than predominantly at the surface. For this argument, we make the plausible assumption that direct interband excitation results in a homogeneous photoexcited carrier density over the cross-section of the tubes, whereas electrons injected from an attached dye would initially be found close to the surfaces. Consequently, if shallow trap states were also predominantly located at the tube surfaces, reduced lifetimes would be expected for injected electrons in dye-sensitized samples. Here, on the contrary, we determine slightly longer lifetimes, which may be the result of a weakly passivating effect of dye-attachment, or simply reflect a superposition of population decay with a finite injection-related rise time component.

THz Charge-Carrier Mobilities in TiO_2 Nanotubes. Early-time THz charge-carrier mobilities of free electrons in TiO_2 nanotubes can be extracted from the photoinduced conductivity under knowledge of the initially absorbed photon density. However, two important potential sources of systematic error have to be mentioned, which can cause an underestimation of the absolute mobility value of nanostructured TiO_2 from the photoinduced THz transmission change. First, the calculation of carrier mobilities from photoconductivity data requires an assumption on the efficiency of incident photon-to-free carrier conversion ϕ (see eq 4) Several possible processes may potentially reduce the photon-to-free-carrier conversion ratio. These include ultrafast immobilization processes, immediate formation of excitonic states,[56] or non-intraband absorption. In the case of dye-sensitized nanotubes, the injection efficiency affects the value of ϕ as well. Hence the values reported here, namely, the effective mobilities $\phi\mu$ represent lower limits to the actual carrier mobility.

Second, because the relative permittivity of TiO_2 is high (bulk anatase THz permittivity: $\epsilon_{bulk} \approx 30$[57,58]) and the characteristic size of the nanostructure is well below the THz wavelength, the bulk of the structure is partly screened from the electric field of the THz wave. This issue has been identified before by Hendry et al.,[12] who employed Maxwell–Garnett effective medium theory to account for electric field screening. Here we perform a numerical calculation to estimate the strength of this effect. Figure 7 shows the 2D-electric field

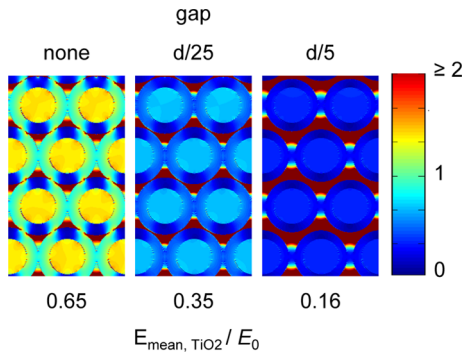

Figure 7. Simulated distribution of the electric-field amplitude in a 2D-cross-section of TiO_2-nanotubes ($\epsilon_r = 30$) surrounded by vacuum ($\epsilon_r = 1$) for three different sizes of the gap x between neighboring tubes with respect to their diameter d ($x = 0$, $x = d/25$, $x = d/5$). Below the colormap plots, the averaged value of the electric field amplitude within the nanotubes normalized to the average electric field across the matrix is stated.

distribution in a cross section of a TiO_2-nanotube array as obtained by numerical integration of Maxwell's equations under the boundary conditions of a given potential difference from north to south. Periodic boundary conditions are applied at the east- and west-ends of the matrix. The results of these calculations show that the extent to which screening reduces the strength of the electric field inside the material is highly dependent on the gap between the tubes. This makes it difficult to obtain a reliable correction factor, as the width of these gaps is hard to determine and not constant along the length of the tubes due to the ripples in the walls observed under the SEM. Finally, we note that for all measurements in this study, the electric field vector of the THz-probe pulse lies in the plane of the nanotube film (i.e., perpendicular to the growth direction), and therefore, the in-plane charge-carrier mobility is obtained. Some degree of anisotropy can however not be ruled out as TiO_2 was found to exhibit a dependence of charge-carrier mobility on direction relative to the crystal axes,[14] and crystallites could possess a preferential orientation with respect to the nanotube structure. Frequency spectra presented in the final section of this article suggest that in-plane localization

DOI: 10.1021/acs.jpcc.5b01827
J. Phys. Chem. C 2015, 119, 9159–9168

effects due to scattering from the surfaces of the nanotubes have at most a small effect on THz conductivity over the investigated frequency range.

We calculate effective electron mobilities using the following expression for the THz conductivity of a thin film of thickness d:[59]

$$\sigma = ne\mu = -\frac{\epsilon_0 c(n_A + n_B)}{d}\left(\frac{\Delta T}{T}\right) \quad (3)$$

Here n_A and n_B are the refractive indices of the materials surrounding the photoexcited film (i.e., in the present case, vacuum and z-cut quartz). The photoexcited carrier concentration n can be determined from the incident photon fluence N_γ/A, if complete photon-to-free-carrier conversion is assumed. To account for the possibility of a photon-to-free-carrier conversion ratio ϕ smaller than unity, we state values of the product $\phi\mu$, referred to as the effective charge-carrier mobility

$$\phi\mu = -\frac{\epsilon_0 c(n_A + n_B)}{(N_\gamma/A)e}\left(\frac{\Delta T}{T}\right) \quad (4)$$

Evaluating several measurements on dye-sensitized samples of all available wall thicknesses, we obtain values for the free-electron effective mobility ranging between $\phi\mu_n = 0.07$ cm^2/(Vs) for the sample anodized at $T_{ano} = 55$ °C (thinnest walls) and $\phi\mu_n = 0.2$ cm^2/(Vs) for the sample anodized at $T_{ano} = 5$ °C (thickest walls). For undyed samples the resulting values are $\phi\mu_n + \phi\mu_p = 0.1$ cm^2/(Vs) for $T_{ano} = 55$ °C and $\phi\mu_n + \phi\mu_p = 0.4$ cm^2/(Vs) for $T_{ano} = 5$ °C, where $\phi\mu_p$ is the effective hole mobility. The discrepancy between the results for dye-sensitized and undyed samples may result from less-than-unity injection efficiencies, the precise value of which is unknown and hence cannot be factored into the mobility calculation. When accounting for electric-field screening based on the performed simulation, the stated values increase by a factor of 1.5 or more depending on the size of the gap between the tube walls. This effect may also be a cause for the variation of the as-measured mobility with anodization temperature consistent with the observation of greater spaces between tubes for higher temperatures.[31]

With regards to the charge extraction performance of TiO_2-nanotubes in dye-sensitized solar cells this study provides two main results. First, it is noted that the THz electron mobilities on TiO_2 nanotubes determined here are similar to those found for sintered TiO_2 nanoparticles ($\phi\mu_{NP} \approx 0.1$ cm^2/(Vs)[13]). Hence electron motion on very short time- and length scales ought to be similarly fast in both materials. Second, however, this study reveals an order of magnitude faster trapping of electrons in shallow traps as a transport-limiting phenomenon in the nanotubes. The fraction of electrons immobilized in photovoltaic devices at any one time can be predicted from the shallow trapping and detrapping rates k_{trap} and k_{detrap}. Considering that deep intraband trap states are expected to be filled under steady state illumination conditions and hence $k_{deep} \approx 0$ (see Figure 6), the equilibrium between shallow trapping and detrapping is reached at $n_{trapped}/n_{free} = k_{trap}/k_{detrap}$ according to eq 1. A fraction of immobilized electrons of $n_{trapped}/(n_{free} + n_{trapped}) \approx 63\%$ is obtained using the values extracted from the data on undyed nanotubes in Figure 2. This is consistent with the observation of a long-lived free electron population in actual dye-sensitized tubes, which is found to consist of about 36% of the initially injected density. In dye-sensitized nanoparticles on the other hand, a near-complete saturation of trap states is observed. The circumstance that only about a third of the injected electrons are available as free carriers in TiO_2-nanotubes reduces the long-range mobility in the material accordingly. Moreover it is noted that trapping events act as a scattering process, which further slows down diffusion. Overall, the observed fast electron trapping provides a plausible explanation for why such TiO_2-nanotubes have so far failed to outperform sintered nanoparticles in terms of charge collection rates despite the existence of more direct percolation paths.

Frequency Dependence of the THz Conductivity. Finally, we recorded photoinduced THz conductivity spectra at early and later time after excitation as shown in Figure 8a for undyed and in Figure 8b for dyed TiO_2 nanotubes. Undyed TiO_2 nanotubes show a predominantly flat response with a negligible imaginary part. The slight drop-off toward low frequency can be attributed to an artifact arising from the diffraction limited THz beam waist approaching the size of the optical pump beam spot. The spectrum is otherwise compatible with Drude-like transport at frequencies below the characteristic relaxation rate ($f \ll 1/\tau$).[60] This stands in contrast to the THz photoconductivity spectra of TiO_2 nanoparticles,[12,13] which exhibit clear localization effects.[61−63] The different behavior may potentially be attributed to the slightly larger "free path" for the electron in the cross section of the nanotubular structure (diameter ∼50 nm) than in the one of the nanoparticle matrix (diameter ∼20 nm), particularly given that the probing electric field primarily penetrates the section of the tube walls tangential to the direction of the field vector, as shown in Figure 7.

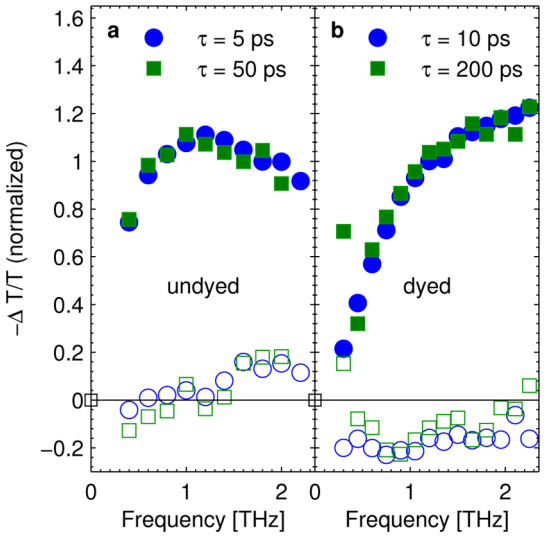

Figure 8. Normalized THz photoconductivity spectra (closed symbols: real part, open symbols: imaginary part). (a) Undyed TiO_2 nanotubes, at early time (5 ps) and at 50 ps after excitation at 266 nm (fluence: 125 μJ/cm^2). (b) Dyed TiO_2 nanotubes, at early time (10 ps) and 200 ps after excitation at 545 nm (Fluence: 680 μJ/cm^2). All spectra taken in vacuum ($p \approx 2 \times 10^{-2}$ mbar). A 450 μm GaP wafer has been used for THz generation in these measurements.

Dye-sensitized nanotubes on the other hand show a very similar THz-conductivity spectrum to nanoparticles, indicating significant localization effects as expressed in the strong decrease of conductivity toward low frequencies and the negative imaginary part leading to a "capacitive" behavior. A reason for the altered spectral response may lie in the spatial

DOI: 10.1021/acs.jpcc.5b01827
J. Phys. Chem. C 2015, 119, 9159−9168

distribution of carriers which is spread out through the bulk for the case of direct excitation in undyed TiO_2 and concentrated at the surfaces for the case of electron injection from a dye. Coulombic interactions with the negatively charged, oxidized dye may strengthen this effect. Other possible explanations may be based on the presence of a (trapped) electron population which has built up over many injection cycles due to the slow back-transfer to the oxidized dye altering the shape of the electric potential within the tubes.

Previously, Richter et al.[56] have reported a resonant feature in the spectra of TiO_2 nanotubes at about 1.8 THz, which they ascribed to an exciton-like state. The authors argue that this state acts as a trap which limits charge-carrier mobility. Such a resonance was not observed in any of the samples here; however, it has to be noted that the growth conditions and the resulting tube dimensions differ significantly between the said study and this work. Richter et al. studied tubes that were approximately 30 times longer and three times larger in diameter compared to those investigated here, which resulted from an at least 25 times longer anodization time. Given that the exciton-like state was linked to an increased concentration of trap states arising from fluorine and titanium impurities, which are introduced during the growth process, differences in the fabrication parameters can plausibly explain the disappearance of the resonance. Alternatively, the resonance may have undergone a sizable frequency-shift to the effect that for our nanotube geometry, it is located outside of the accessible spectral range of the experimental setup. If it can be confirmed that such an exitonic state is in fact present in nanotubes films of the type studied here, it may well be conceivable that the physical origin of the fast charge-carrier trapping we observe is linked to this state. Further experimental work beyond the scope of the present study is required to test this hypothesis.

CONCLUSION

In conclusion, we studied the decay dynamics of photoexcited and of injected free electrons in TiO_2 nanotubes by means of optical-pump-terahertz-probe spectroscopy. The results may be described within a simple model of shallow trapping, detrapping from shallow traps, and irreversible immobilization of electrons in deep traps. Interestingly, we find shallow trapping lifetimes to be as short as a few tens of picoseconds making the decay process at least an order of magnitude faster than in sintered TiO_2 nanoparticles. This provides a possible explanation for why the charge-collection performance of TiO_2 nanotubes in dye-sensitized solar cells has not so far surpassed that of TiO_2-nanoparticles despite their more direct electron percolation paths. A comparison of nanotube samples that were anodized at different temperatures and therefore have different wall thicknesses showed no significant influence of this parameter on charge-carrier lifetimes. Similarly, we observed fast trapping dynamics upon direct interband excitation of the material and upon injection from an attached dye. These results suggest that there is no predominantly high concentration of shallow traps at the surface of the tubes. We revealed that while trap-filling effects can almost completely eliminate charge-carrier decay on the nanosecond time scale in dye-sensitized nanoparticles, no saturation effects are observed for the shallow traps in nanotubes. Effective early time carrier mobilities were found to be similar in both materials with values on the order of 0.1 $cm^2/(Vs)$. We note that due to electric field screening effects, this value represents a lower limit with the actual electron mobilities expected to be higher by at least a factor 1.5. In view of device applications, the results from this work suggest that potential improvements to the charge transport performance of TiO_2 nanotubes may be achieved, if modifications to the anodization process can be identified that reduce the concentration of incorporated trap states.

AUTHOR INFORMATION

Corresponding Author

*E-mail: l.herz@physics.ox.ac.uk. Phone: +44-1865-272200.

Present Address

‡Technische Universität München, Physik-Department, Lehrstuhl für Funktionelle Materialien, James-Franck-Str. 1, 85747 Garching, Germany.

Notes

The authors declare no competing financial interest.

ACKNOWLEDGMENTS

The authors gratefully acknowledge funding from the Engineering and Physical Sciences Research Council (EPSRC).

REFERENCES

(1) Linsebigler, A. L.; Lu, G.; Yates, J. T. Photocatalysis on TiO_2 Surfaces: Principles, Mechanisms, and Selected Results. *Chem. Rev.* **1995**, *95*, 735−758.

(2) Tang, Y.; Zhang, Y.; Deng, J.; Wei, J.; Tam, H. L.; Chandran, B. K.; Dong, Z.; Chen, Z.; Chen, X. Mechanical Force-Driven Growth of Elongated Bending TiO_2-based Nanotubular Materials for Ultrafast Rechargeable Lithium Ion Batteries. *Adv. Mater.* **2014**, *26*, 6111−6118.

(3) Bach, U.; Lupo, D.; Comte, P.; Moser, J.-E.; Weissortel, F.; Salbeck, J.; Spreitzer, H.; Grätzel, M. Solid-state Dye-sensitized Mesoporous TiO_2 Solar Cells with High Photon-to-Electron Conversion Efficiencies. *Nature* **1998**, *395*, 583.

(4) Roy, P.; Berger, S.; Schmuki, P. TiO_2 Nanotubes: Synthesis and Applications. *Angew. Chem., Int. Ed.* **2011**, *50*, 2904−2939.

(5) Dittrich, T.; Lebedev, E.; Weidmann, J. Electron Drift Mobility in Porous TiO_2 (Anatase). *Phys. Status Solidi A* **1998**, *165*, R5−R6.

(6) Yella, A.; Lee, H.-W.; Tsao, H. N.; Yi, C.; Chandiran, A. K.; Nazeeruddin, M.; Diau, E. W.-G.; Yeh, C.-Y.; Zakeeruddin, S. M.; Grätzel, M. Porphyrin-Sensitized Solar Cells with Cobalt (II/III)-Based Redox Electrolyte Exceed 12% Efficiency. *Science* **2011**, *334*, 629−634.

(7) Tiwana, P.; Docampo, P.; Johnston, M. B.; Snaith, H. J.; Herz, L. M. Electron Mobility and Injection Dynamics in Mesoporous ZnO, SnO_2, and TiO_2 Films Used in Dye-Sensitized Solar Cells. *ACS Nano* **2011**, *5*, 5158.

(8) Forro, L.; Chauvet, O.; Emin, D.; Zuppiroli, L.; Berger, H.; Levy, F. High Mobility n-type Charge Carriers in Large Single Crystals of Anatase TiO_2. *J. Appl. Phys.* **1994**, *75*, 633−635.

(9) Dunn, H. K.; Peter, L. M. How Efficient Is Electron Collection in Dye-Sensitized Solar Cells? Comparison of Different Dynamic Methods for the Determination of the Electron Diffusion Length. *J. Phys. Chem. C* **2009**, *113*, 4726−4731.

(10) Krüger, J.; Plass, R.; Grätzel, M.; Cameron, P. J.; Peter, L. M. Charge Transport and Back Reaction in Solid-State Dye-Sensitized Solar Cells: A Study Using Intensity-Modulated Photovoltage and Photocurrent Spectroscopy. *J. Phys. Chem. B* **2003**, *107*, 7536−7539.

(11) Jennings, J. R.; Peter, L. M. A Reappraisal of the Electron Diffusion Length in Solid-State Dye-Sensitized Solar Cells. *J. Phys. Chem. C* **2007**, *111*, 16100−16104.

(12) Hendry, E.; Koeberg, M.; O'Regan, B.; Bonn, M. Local Field Effects on Electron Transport in Nanostructured TiO_2 Revealed by Terahertz Spectroscopy. *Nano Lett.* **2006**, *6*, 755.

(13) Tiwana, P.; Parkinson, P.; Johnston, M. B.; Snaith, H. J.; Herz, L. M. Ultrafast Terahertz Conductivity Dynamics in Mesoporous TiO_2: Influence of Dye Sensitization and Surface Treatment in Solid-

DOI: 10.1021/acs.jpcc.5b01827
J. Phys. Chem. C 2015, 119, 9159−9168

state Dye-sensitized Solar Cells. *J. Phys. Chem. C* **2010**, *114*, 1365−1371.
(14) Hendry, E.; Wang, F.; Shan, J.; Heinz, T. F.; Bonn, M. Electron Transport in TiO_2 Probed by THz time-Domain Spectroscopy. *Phys. Rev. B* **2004**, *69*, 081101.
(15) Turner, G. M.; Beard, M. C.; Schmuttenmaer, C. A. Carrier Localization and Cooling in Dye-sensitized Nanocrystalline Titanium Dioxide. *J. Phys. Chem. B* **2002**, *106*, 11716.
(16) Paulose, M.; Shankar, K.; Varghese, O.; Mor, G.; Grimes, C. Application of Highly-ordered TiO_2 Nanotube-Arrays In Heterojunction Dye-sensitized Solar Cells. *J. Phys. D* **2006**, *39*, 2498−2503.
(17) Jennings, J. R.; Ghicov, A.; Peter, L. M.; Schmuki, P.; Walker, A. B. Dye-sensitized Solar Cells Based On Oriented TiO_2 Nanotube Arrays: Transport, Trapping, and Transfer of Electrons. *J. Am. Chem. Soc.* **2008**, *130*, 13364−13372.
(18) Docampo, P.; Ivaturi, A.; Gunning, R.; Diefenbach, S.; Kirkpatrick, J.; Palumbiny, C. M.; Sivaram, V.; Geaney, H.; Schmidt-Mende, L.; Welland, M. E.; et al. The Influence of 1D, Meso- and Crystal Structures on Charge Transport and Recombination in Solid-state Dye-sensitized Solar Cells. *J. Mater. Chem. A* **2013**, *1*, 12088−12095.
(19) Gong, D.; Grimes, C.; Varghese, O.; Hu, W.; Singh, R.; Chen, Z.; Dickey, E. Titanium Oxide Nanotube Arrays Prepared by Anodic Oxidation. *J. Mater. Res.* **2001**, *16*, 3331−3334.
(20) Zhu, K.; Neale, N. R.; Miedaner, A.; Frank, A. J. Enhanced Charge-Collection Efficiencies and Light Scattering in Dye-sensitized Solar Cells Using Oriented TiO_2 Nanotubes Arrays. *Nano Lett.* **2007**, *7*, 69−74.
(21) Beard, M. C.; Turner, G. M.; Schmuttenmaer, C. A. Terahertz Spectroscopy. *J. Phys. Chem. B* **2002**, *106*, 7146.
(22) Parkinson, P.; Lloyd-Hughes, J.; Gao, Q.; Tan, H. H.; Jagadish, C.; Johnston, M. B.; Herz, L. M. Transient Terahertz Conductivity of GaAs Nanowires. *Nano Lett.* **2007**, *7*, 2162−2165.
(23) Nvemec, H.; Kužel, P.; Sundström, V. Charge Transport in Nanostructured Materials for Solar Energy Conversion Studied by Time-resolved Terahertz Spectroscopy. *J. Photochem. Photobiol., A* **2010**, *215*, 123−139.
(24) Docampo, P.; Tiwana, P.; Sakai, N.; Miura, H.; Herz, L.; Murakami, T.; Snaith, H. J. Unraveling the Function of an MgO Interlayer in Both Electrolyte and Solid-State SnO_2 Based Dye-Sensitized Solar Cells. *J. Phys. Chem. C* **2012**, *116*, 22840.
(25) Tiwana, P.; Docampo, P.; Johnston, M. B.; Herz, L. M.; Snaith, H. J. The Origin of an Efficiency Improving "Light Soaking" Effect in SnO_2 Based Solid-State Dye-sensitized Solar Cells. *Energy Environ. Sci.* **2012**, *5*, 9566.
(26) Tang, H.; Berger, H.; Schmid, P.; Levy, F.; Burri, G. Photoluminescence in TiO_2 Anatase Single-Crystals. *Solid State Commun.* **1993**, *87*, 847−850.
(27) Reddy, K. M.; Manorama, S. V.; Reddy, A. R. Bandgap Studies on Anatase Titanium Dioxide Nanoparticles. *Mater. Chem. Phys.* **2003**, *78*, 239−245.
(28) Liu, H.; Yao, J.; Puri, A. Second and Third Harmonic Generation in BBO by Femtosecond Ti:Sapphire Laser Pulses. *Opt. Commun.* **1994**, *109*, 139−144.
(29) Berger, S.; Hahn, R.; Roy, P.; Schmuki, P. Self-organized TiO_2 Nanotubes: Factors Affecting Their Morphology and Properties. *Phys. Status Solidi B* **2010**, *247*, 2424−2435.
(30) Beranek, R.; Hildebrand, H.; Schmuki, P. Self-Organized Porous Titanium Oxide Prepared in H_2SO_4/HF Electrolytes. *Electrochem. Solid-State Lett.* **2003**, *6*, B12−B14.
(31) Weickert, J.; Palumbiny, C.; Nedelcu, M.; Bein, T.; Schmidt-Mende, L. Controlled Growth of TiO_2 Nanotubes on Conducting Glass. *Chem. Mater.* **2011**, *23*, 155−162.
(32) Kroeze, J. E.; Savenije, T. J.; Warman, J. M. Contactless Determination of the Efficiency of Photo-induced Charge Separation in a Porphyrin-TiO_2 Bilayer. *J. Photochem. Photobiol., A* **2002**, *148*, 49−55.
(33) Jepsen, P. U.; Schairer, W.; Libon, I. H.; Lemmer, U.; Hecker, N. E.; Birkholz, M.; Lips, K.; Schall, M. Ultrafast Carrier Trapping in Microcrystalline Silicon Observed in Optical Pump-Terahertz Probe Measurements. *Appl. Phys. Lett.* **2001**, *79*, 1291−1293.
(34) Bauer, C.; Boschloo, G.; Mukhtar, E.; Hagfeldt, A. Ultrafast Relaxation Dynamics of Charge Carriers Relaxation in ZnO Nanocrystalline Thin Films. *Chem. Phys. Lett.* **2004**, *387*, 176−181.
(35) Cooke, D. G.; Hegmann, F. A.; Mazur, Y. I.; Wang, Z. M.; Black, W.; Wen, H.; Salamo, G. J.; Mishima, T. D.; Lian, G. D.; Johnson, M. B. Ultrafast Carrier Capture Dynamics in InGaAs/GaAs Quantum Wires. *J. Appl. Phys.* **2008**, *103*, 023710.
(36) Fekete, L.; Kužel, P.; Němec, H.; Kadlec, F.; Dejneka, A.; Stuchlík, J.; Fejfar, A. Ultrafast Carrier Dynamics in Microcrystalline Silicon Probed by Time-resolved Terahertz Spectroscopy. *Phys. Rev. B* **2009**, *79*, 115306.
(37) Wang, X.; Feng, Z.; Shi, J.; Jia, G.; Shen, S.; Zhou, J.; Li, C. Trap States and Carrier Dynamics of TiO_2 Studied by Photoluminescence Spectroscopy under Weak Excitation Condition. *Phys. Chem. Chem. Phys.* **2010**, *12*, 7083−7090.
(38) Zhao, H.; Zhang, Q.; Weng, Y.-X. Deep Surface Trap Filling by Photoinduced Carriers and Interparticle Electron Transport Observed in TiO_2 Nanocrystalline Film with Time-Resolved Visible and Mid-IR Transient Spectroscopies. *J. Phys. Chem. C* **2007**, *111*, 3762−3769.
(39) Munnix, S.; Schmeits, M. Origin of Defect States on the Surface of TiO_2. *Phys. Rev. B* **1985**, *31*, 3369−3371.
(40) Diebold, U. The Surface Science of Titanium Dioxide. *Surf. Sci. Rep.* **2003**, *48*, 53−229.
(41) Wu, P.-G.; Ma, C.-H.; Shang, J. Effects of Nitrogen Doping on Optical Properties of TiO_2 Thin Films. *Appl. Phys. A: Mater. Sci. Process.* **2005**, *81*, 1411−1417.
(42) Joyce, H. J.; Wong-Leung, J.; Yong, C.; Docherty, C. J.; Paiman, S.; Gao, Q.; Tan, H. H.; Jagadish, C.; Lloyd-Hughes, J.; Herz, L. M.; et al. Ultra-low Surface Recombination Velocity in InP Nanowires Probed by Terahertz Spectroscopy. *Nano Lett.* **2012**, *12*, 5325−5330.
(43) Joyce, H. J.; Docherty, C. J.; Gao, Q.; Tan, H. H.; Jagadish, C.; Lloyd-Hughes, J.; Herz, L. M.; Johnston, M. B. Electronic Properties of GaAs, InAs and InP Hanowires Studied by Terahertz Spectroscopy. *Nanotechnology* **2013**, *24*, 214006.
(44) Ruan, C.; Paulose, M.; Varghese, O. K.; Grimes, C. A. Enhanced Photoelectrochemical-Response in Highly Ordered TiO_2 Nanotube-Arrays Anodized in Boric Acid Containing Electrolyte. *Sol. Energy Mater. Sol. C* **2006**, *90*, 1283−1295.
(45) Marino, C. E.; Nascente, P. A.; Biaggio, S. R.; Rocha-Filho, R. C.; Bocchi, N. XPS Characterization of Anodic Titanium Oxide Films Grown in Phosphate Buffer Solutions. *Thin Solid Films* **2004**, *468*, 109−112.
(46) Dittrich, T.; Weidmann, J.; Koch, F.; Uhlendorf, I.; Lauermann, I. Temperature- and Oxygen Partial Pressure-Dependent Electrical Conductivity in Nanoporous Rutile and Anatase. *Appl. Phys. Lett.* **1999**, *75*, 3980−3982.
(47) Varghese, O.; Gong, D.; Paulose, M.; Ong, K.; Dickey, E.; Grimes, C. Extreme Changes in the Electrical Resistance of Titania Nanotubes with Hydrogen Exposure. *Adv. Mater.* **2003**, *15*, 624−627.
(48) Fujishima, A.; Zhang, X.; Tryk, D. A. TiO_2 Photocatalysis and Related Surface Phenomena. *Surf. Sci. Rep.* **2008**, *63*, 515−582.
(49) Thompson, T.; Yates, J. TiO_2-based Photocatalysis: Surface Defects, Oxygen and Charge Transfer. *Top. Catal.* **2005**, *35*, 197−210.
(50) Westermark, K.; Henningsson, A.; Rensmo, H.; Södergren, S.; Siegbahn, H.; Hagfeldt, A. Determination of the Electronic Density of States at a Nanostructured TiO_2/Ru-dye/Electrolyte Interface by Means of Photoelectron Spectroscopy. *Chem. Phys.* **2002**, *285*, 157−165.
(51) Sekiya, T.; Yagisawa, T.; Kamiya, N.; Das Mulmi, D.; Kurita, S.; Murakami, Y.; Kodaira, T. Defects in Anatase TiO_2 Single Crystal Controlled by Heat Treatments. *J. Phys. Soc. Jpn.* **2004**, *73*, 703−710.
(52) Desilvestro, J.; Grätzel, M.; Kavan, L.; Moser, J.; Augustynski, J. Highly Efficient Sensitization of Titanium-dioxide. *J. Am. Chem. Soc.* **1985**, *107*, 2988−2990.
(53) Cao, F.; Oskam, G.; Meyer, G.; Searson, P. Electron Transport in Porous Nanocrystalline TiO_2 Photoelectrochemical Cells. *J. Phys. Chem.* **1996**, *100*, 17021−17027.

DOI: 10.1021/acs.jpcc.5b01827
J. Phys. Chem. C 2015, 119, 9159−9168

(54) Kopidakis, N.; Benkstein, K. D.; van de Lagemaat, J.; Frank, A. J. Transport-Limited Recombination of Photocarriers in Dye-Sensitized Nanocrystalline TiO_2 Solar Cells. *J. Phys. Chem. B* **2003**, *107*, 11307−11315.
(55) Schwarzburg, K.; Willig, F. Influence of Trap Filling on Photocurrent Transients in Polycrystalline TiO_2. *Appl. Phys. Lett.* **1991**, *58*, 2520−2522.
(56) Richter, C.; Schmuttenmaer, C. A. Exciton-like Trap States Limit Electron Mobility in TiO_2 Nanotubes. *Nat. Nanotechnol.* **2010**, *5*, 769−772.
(57) Roberts, S. Dielectric Constants and Polarizabilities of Ions in Simple Crystals and Barium Titanate. *Phys. Rev.* **1949**, *76*, 1215−1220.
(58) Gonzalez, R. J.; Zallen, R.; Berger, H. Infrared Reflectivity and Lattice Fundamentals in Anatase TiO_2. *Phys. Rev. B* **1997**, *55*, 7014−7017.
(59) Nienhuys, H.-K.; Sundström, V. Intrinsic Complications in the Analysis of Optical-Pump, Terahertz Probe Experiments. *Phys. Rev. B* **2005**, *71*, 235110.
(60) Lloyd-Hughes, J.; Jeon, T.-I. A Review of the Terahertz Conductivity of Bulk and Nano-Materials. *J. Infrared Millim. Terahertz Waves* **2012**, *33*, 871−925.
(61) Smith, N. V. Classical Generalization of the Drude Formula for the Optical Conductivity. *Phys. Rev. B* **2001**, *64*, 155106.
(62) Němec, H.; Kužel, P.; Sundström, V. Far-infrared Response of Free Charge Carriers Localized in Semiconductor Nanoparticles. *Phys. Rev. B* **2009**, *79*, 115309.
(63) Kužel, P.; Němec, H. Terahertz Conductivity in Nanoscaled Systems: Effective Medium Theory Aspects. *J. Phys. D-Appl. Phys.* **2014**, *47*, 374005.

DOI: 10.1021/acs.jpcc.5b01827
J. Phys. Chem. C 2015, 119, 9159−9168